THE JOURNAL OF BIOLOGICAL CHEMISTRY VOL. 282, NO. 11, pp. 8044–8051, March 16, 2007

A Cation-π Interaction Discriminates among Sodium Channels That Are Either Sensitive or Resistant to Tetrodotoxin Block*

Received for publication, December 11, 2006, and in revised form, January 11, 2007 Published, JBC Papers in Press, January 19, 2007, DOI 10.1074/jbc.M611334200

Vincent P. Santarelli[‡], Amy L. Eastwood[§], Dennis A. Dougherty[§], Richard Horn[‡], and Christopher A. Ahern[‡1]

From the [‡]Department of Molecular Physiology and Biophysics, Institute of Hyperexcitability, Jefferson Medical College, Philadelphia, Pennsylvania 19107 and the [§]Division of Chemistry and Chemical Engineering, California Institute of Technology, Pasadena, California 91125

Voltage-gated sodium channels control the upstroke of the action potential in excitable cells of nerve and muscle tissue, making them ideal targets for exogenous toxins that aim to squelch electrical excitability. One such toxin, tetrodotoxin (TTX), blocks sodium channels with nanomolar affinity only when an aromatic Phe or Tyr residue is present at a specific location in the external vestibule of the ion-conducting pore. To test whether TTX is attracted to Tyr^{401} of $Na_V1.4$ through a cation-π interaction, this aromatic residue was replaced with fluorinated derivatives of Phe using *in vivo* nonsense suppression. Consistent with a cation-π interaction, increased fluorination of Phe^{401}, which reduces the negative electrostatic potential on the aromatic face, caused a monotonic increase in the inhibitory constant for block. Trifluorination of the aromatic ring decreased TTX affinity by ~50-fold, a reduction similar to that caused by replacement with the comparably hydrophobic residue Leu. Furthermore, we show that an energetically equivalent cation-π interaction underlies both use-dependent and tonic block by TTX. Our results are supported by high level *ab initio* quantum mechanical calculations applied to a model of TTX binding to benzene. Our analysis suggests that the aromatic side chain faces the permeation pathway where it orients TTX optimally and interacts with permeant ions. These results are the first of their kind to show the incorporation of unnatural amino acids into a voltage-gated sodium channel and demonstrate that a cation-π interaction is responsible for the obligate nature of an aromatic at this position in TTX-sensitive sodium channels.

Sodium channels control electrical excitability in muscle and nervous tissues by driving membrane depolarization during an action potential. These large (~260 kDa) proteins have four homologous transmembrane domains that are arranged in a clockwise orientation around a central pore (1). Numerous sodium channel isoforms exist and share the common traits of being exceptionally sensitive to voltage and selective for Na^+ ions (2). They can, however, differ in expression patterns, inactivation time course, sensitivity to toxins, and effects of auxiliary subunits. In terms of extracellular block by the guanidinium toxin tetrodotoxin (TTX),[2] sodium channels have been deemed binary in their sensitivity; they are either TTX-sensitive, blocked by low nanomolar concentrations, or TTX-resistant with blocking constants in the micromolar range (3). Members of the former class include isoforms expressed in brain ($Na_V1.1$, $Na_V1.2$, and $Na_V1.3$), skeletal muscle ($Na_V1.4$), and peripheral nervous system ($Na_V1.6$ and $Na_V1.7$); the latter class includes isoforms of cardiac muscle ($Na_V1.5$) and sensory neurons ($Na_V1.8$ and $Na_V1.9$). A number of point mutations in the external vestibule of the channel can substantially disrupt TTX binding (4–8), yet many of these residues are conserved between sensitive and resistant isoforms and therefore cannot explain isoform-specific TTX sensitivity. It has been established, however, that a single aromatic residue conserved in the first homologous domain (DI) of TTX-sensitive isoforms underlies isoform-specific block (9–11). Mutagenic replacement of this aromatic residue, Tyr^{401} in the rat skeletal muscle sodium channel $Na_V1.4$, with the homologous residue from $Na_V1.5$, a cysteine, renders this isoform insensitive to TTX (10, 11). More importantly, a high affinity TTX site with nanomolar affinity can be generated in $Na_V1.5$ upon a single aromatic substitution at this site (9, 10), confirming the importance for TTX block of Phe or Tyr at this position.

Many pore blockers mimic a channel permeant ion and occlude conduction by taking its place in the permeation pathway. In the present example, the charged guanidinium moiety of TTX may replace sodium at the external mouth of the channel. Therefore an understanding of block by TTX and other guanidinium toxins holds the promise of providing insight into the molecular architecture of the permeation pathway. The sodium channel selectivity filter has been hypothesized to be formed in part by the side chains of Asp, Glu, Lys, and Ala, one from each of the four homologous domains, DI–DIV, respectively (12, 13). The DEKA locus is assisted by an outer ring of negative charges that electrostatically focus sodium ions toward the mouth of the selectivity filter (14, 15). Mutation of residues in either the inner or outer ring decrease TTX affinity and alter single channel conductance (5, 16), suggesting that the TTX binding site overlaps with the extracellular entrance of the

* This work was supported by Grants GM079427 and NS34407 from the National Institutes of Health. The costs of publication of this article were defrayed in part by the payment of page charges. This article must therefore be hereby marked "*advertisement*" in accordance with 18 U.S.C. Section 1734 solely to indicate this fact.

[1] To whom correspondence should be addressed. Tel.: 215-503-6721; Fax: 215-503-2073; E-mail: Christopher.Ahern@jefferson.edu.

[2] The abbreviations used are: TTX, tetrodotoxin; aa, amino acids; NVOC, nitroveratryloxycarbonyl; WT, wild type.

permeation pathway. The aromatic residue of interest for the current work, Tyr^{401} in $Na_V1.4$, is located between the two aforementioned charged rings, and its replacement with cysteine reduces single channel conductance (10), further suggesting a role for this site in sodium permeation. The homologous residue in the TTX-resistant cardiac isoform $Na_V1.5$, a cysteine, underlies sensitivity to extracellular pore block by heavy metals (11, 17).

An aromatic side chain may interact with a large organic cation like TTX through a combination of forces, including an induced dipole in the toxin and the aromatic, donor-acceptor, charge-transfer, and dispersion forces, as well as hydrophobic effects (18). Electrostatic energy may also be provided by the attraction between the negative electrostatic potential on the face of the aromatic ring and the guanidinium moiety of TTX, an affinity termed the cation-π interaction (18, 19). This possibility was suggested previously to account for the importance of an aromatic residue in TTX block (9, 20).

Traditional site-directed mutagenesis is not helpful in discriminating among the many energetic components of binding, because outright amino acid substitution tends to change hydrophobicity, structure, polarizability, and electrostatics concurrently. These shortcomings are readily averted by employing *in vivo* nonsense suppression to incorporate unnatural amino acids with subtle structural changes (21). This method has been used previously to test for cation-π interactions by incorporating a series of progressively fluorinated aromatic derivatives into the ligand binding pockets of a variety of ion channels (22–25). We have also used this approach to explore extracellular block of potassium channels by cationic tetraethylammonium (26). The principle underlying this strategy is simple. Each fluorine atom substitution progressively reduces the negative electrostatic potential on the face of the aromatic, thereby reducing the electrostatic component of binding affinity. For studies of this kind, unnatural amino acids are clearly superior to their traditional counterparts. Serial fluorination does not substantially change the size, shape, polarizability, or hydrophobicity of the aromatic side chain (18, 27), so any loss in binding energy is caused by cation-π electrostatics.

In the present study, we used the *in vivo* nonsense suppression method to introduce a series of progressively fluorinated Phe residues at position 401 in $Na_V1.4$ and assayed the resulting channels for their sensitivity to TTX. Stepwise fluorination monotonically increased the equilibrium binding constant, as observed in other known organic cation-π systems. Furthermore, complete neutralization of the negative electrostatic potential of the aromatic face by trifluorination of the aromatic side chain resulted in a TTX block that was similar to replacement of Phe^{401} by Leu, suggesting that hydrophobicity alone cannot explain high affinity block. Analysis of the blocking kinetics reveals that withdrawal of π electrons from the aromatic face of Phe^{401} is manifested primarily as a decrease in the association rate constant for TTX block. These results demonstrate that Phe^{401} interacts with TTX through a substantial cation-π interaction which, along with other energetic contributions, supports high affinity block in TTX-sensitive isoforms.

EXPERIMENTAL PROCEDURES

Molecular Biology and Unnatural Amino Acids—The channel we used, $rNa_V1.4$-pBSTA, was a gift from Drs. Baron Chanda and Francisco Bezanilla. The *in vivo* nonsense suppression methodology was performed as described previously (26, 28). Tyr^{401} of the $Na_V1.4$ cDNA was mutated into a TAG nonsense (stop) codon by conventional mutagenesis (Stratagene), and complementary mRNA was transcribed from this cDNA (mMessage mMachine, Ambion). Unnatural amino acids (aa) were protected with nitroveratryloxycarbonyl (NVOC), activated as the cyanomethyl ester, coupled to the dinucleotide dCA, and then ligated to a modified tRNA from *Tetrahymena thermophila*. This tRNA contains the complementary anticodon to the UAG stop site within the $Na_V1.4$-Y401UAG cRNA. Deprotection of the aminoacylated tRNA-aa was performed by UV irradiation immediately before injection into Stage V–VI *Xenopus* oocytes. Typically, 20 ng of tRNA-aa, 25 ng of $Na_V1.4$-401UAG cRNA, and 2 ng of sodium channel β_1-subunit cRNA (29) were co-injected in a 50-nl volume into each oocyte.

The present study employed phenylalanine amino acid derivatives with one, two or three appended fluorines termed $3F_1$-Phe (single fluorination at the 3 position), $3,5F_2$-Phe (fluorination at the 3 and 5 positions), $3,4,5F_3$-Phe (fluorination at the 3, 4, and 5 positions). For clarity we refer to the monofluorinated derivative at the *meta* position as $3F_1$-Phe. However, it is possible that the fluorine may occupy the 3 or the 5 position depending on incorporation stereochemistry.

Electrophysiology and Analysis—Whole oocyte sodium current was recorded with the two-microelectrode voltage clamp technique using an OC-725C voltage clamp (Warner Instruments, Hamden, CT) in a standard Ringers solution (in mM): 116 NaCl, 2 KCl, 1 $MgCl_2$, 0.5 $CaCl_2$, 5 HEPES, pH 7.5. Recording electrodes were filled with a 3 M KCl solution and had a resistance equal to or less than 1 MΩ. Perfusion experiments were performed with an ALA VM8 (ALA Scientific) gravity-flow delivery system. A TTX stock (1 mM in H_2O) was stored at −20 °C. TTX working dilutions were made fresh each day from this stock. Inhibitory constants (K_i) of the resting and stimulated channels were obtained using a 2-Hz protocol (100 pulses of 10-ms duration to −10 mV from a holding potential of −100 mV) after a quiescent period of 3 min. The first pulse in this train assays the resting (tonic) block by TTX, and the 100th pulse elicits stimulated block (Fig. 4*A*). The time course of TTX dissociation (washoff) was obtained by exposing the oocyte to a TTX concentration producing block in the range of 30–75%, and stimulated at 2 Hz. Once the high affinity stimulated state was achieved, perfusion was switched to a TTX-free bath solution and washout was observed as an exponential increase in peak current.

The time course and extent of use-dependent block were analyzed according a previously established framework (7, 30, 31). Three rate constants underlying toxin block were estimated, as well as two inhibitory constants for each mutation at position 401. The tonic (low affinity) and stimulated (high affinity) states have dissociation rate constants of k_{off}^{L} and k_{off}^{H}, respectively. A single association rate constant k_{on} applies to

TABLE 1

Theoretical binding energies of TTX with fluorinated derivatives of benzene

Calculations are described under "Experimental Procedures." The geometry and orientation of TTX binding was set by a gas-phase optimization, followed by aligning TTX with the structure in Fig. 6 to know which positions to fluorinate. All values are in kcal/mol. ΔE is the binding energy of TTX to the benzene derivatives (F_n-Benzene, where n = number of fluorines) calculated in the gas phase. The energy caused by monofluorination (F_1-Benzene) was calculated from the average energies of $3F_1$-Benzene and $5F_1$-Benzene, which differed because of the asymmetric structure of TTX (Fig. 6). The hydration energies for TTX, benzene derivatives, and the TTX-benzene complex were calculated using a Poisson-Boltzmann equation solver. ΔG_{solv} is the change in solvation free energy caused by TTX binding to the benzene derivative. $\Delta G_{binding} = \Delta E + \Delta G_{solv}$ is the Gibbs free energy of TTX binding, and $\Delta\Delta G$ is the effect of fluorination on TTX binding.

	ΔE (gas)	Hydration Energies			ΔG_{solv}	$\Delta G_{binding}$	$\Delta\Delta G$
		TTX	F_n-Benzene	Complex			
F_0-Benzene	−7.91	−89.88	−1.59	−77.87	13.6	5.69	0
F_1-Benzene	−5.14	−89.88	−2.09	−79.95	12.02	6.88	1.19
$3,5F_2$-Benzene	−2.14	−89.88	−2.22	−81.51	10.59	8.45	2.76
$3,4,5F_3$-Benzene	0.14	−89.88	−2.79	−82.96	9.71	9.85	4.16

TABLE 2

Affinity and kinetics of TTX block in tonic and stimulated states

Rate constants (k^H_{off}, k^L_{off}, and k_{on}) and equilibrium inhibitory constants (K^L_i and K^H_i) were determined as described under "Experimental Procedures." The number of cells is enclosed in parentheses.

	K^L_i Tonic	K^H_i Stim	k^L_{off} Tonic	k^H_{off} Stim	k_{on}
	nM	nM	s^{-1}	s^{-1}	$s^{-1}\ \mu M^{-1}$
WT (Tyr^{401})	19 ± 6 (5)	6 ± 1 (5)	0.13 ± .04 (5)	0.037 ± .002 (4)	6.84 ± 0.79 (9)
Y401F	25 ± 2 (4)	5 ± 0.9 (4)	0.161 ± 0.017 (4)	0.033 ± 0.001 (4)	6.58 ± 0.17 (4)
Phe[a]	25 ± 3 (6)[a]	7 ± 0.9 (6)[a]	0.1545 ± 0.0128 (6)[a]	0.040 ± 0.004 (5)[a]	6.13 ± 1.04 (6)[a]
$3F_1$-Phe[a]	49 ± 7 (6)[a]	10 ± 1 (6)[a]	0.208 ±0.032 (5)[a]	0.040 ± 0.002 (5)[a]	4.08 ± 0.46 (5)[a]
$3,5F_2$-Phe[a]	316 ± 32 (6)[a]	93 ± 9 (6)[a]	0.642 ± 0.064 (6)[a]	0.181 ± 0.019 (6)[a]	2.04 ± 0.27 (6)[a]
$3,4,5F_3$-Phe[a]	974 ± 61 (6)[a]	350 ± 28 (6)[a]	0.352 ± 0.022 (6)[a]	0.134 ± 0.032 (6)[a]	0.361 ± 0.058 (6)[a]
Y401L	2070 ± 223 (6)	1006 ± 104 (6)	0.363 ± 0.082 (4)	0.171 ± 0.031 (4)	0.209 ± 0.052 (4)
Y401C	108,000 ± 14,000 (4)	108,000 ± 14,000 (4)			

[a] These mutants were generated by nonsense suppression.

both states, because dissociation of the toxin from the channel is assumed to cause a rapid conversion of all channels to the low affinity state (30). The two inhibitory constants K^L_i and K^H_i were estimated from the fraction of TTX block before and after 2-Hz stimulation, respectively, using fits to dose-response curves of block, except for the natural mutant Y401C, where the effect of a single [TTX] was used to estimate K^L_i and K^H_i. The rate constant k^H_{off} is the inverse of the time constant of washoff during high-frequency stimulation, k_{on} is estimated as the ratio k^H_{off}/K^H_i, and k^L_{off} is the product $k_{on}K^L_i$.

Free Energy Computations—For *ab initio*, molecular mechanics, and mixed-mode calculations, respectively, we used the programs Jaguar and MacroModel and QSite. The structure of the monovalent cation TTX was optimized at the HF/6-31G**++ level (Fig. 1*A*). The electrostatic potential at the surface of hydrated TTX (Fig. 1*B*) was determined using a self-consistent reaction field method with the Poisson-Boltzmann solver in Jaguar. The energetic consequences of fluorinating the aromatic ring on TTX binding were calculated as follows. We first optimized the geometry for binding of TTX to benzene at the HF/6-31G*++ level in the gas phase. This geometry was maintained for all fluorinated derivatives of benzene. We then computed the Gibbs free energy of TTX binding at the HF/6-31G**++ level, accounting both for the gas-phase *ab initio* energies, as well as the energies of hydration, using the aforementioned Poisson-Boltzmann solver (Table 1; for example, see Ref. 32). No correction was made for basis set superposition error.

To determine the geometry of the TTX-bound intermediate of Fig. 6, we used the molecular model of Lipkind and Fozzard (33) for the outer mouth of the sodium channel pore. TTX bound to benzene, optimized at the quantum mechanical level, was aligned with the aromatic ring of Tyr^{401}. The TTX-benzene complex can be oriented in 6 ways due to the 6-fold symmetry of the aromatic ring. Of these, we chose the minimum energy conformation determined by MacroModel using the OPLS2005 force field (34). This structure was further refined by a mixed-mode Quantum Mechanics/Molecular Mechanics (QM/MM) optimization in which the Tyr^{401} side chain and TTX were treated at the QM level (HF/6–31G*), and the rest of the structure was treated at the MM level (OPLS2001 force field) with water represented as a continuum. For this calculation TTX and the Tyr^{401} side chain were free to move, but the coordinates of all other atoms of the channel were fixed.

RESULTS

TTX affinity is nearly three orders of magnitude higher in TTX-sensitive sodium channels than in TTX-resistant isoforms, a difference that has been attributed to the lack of an aromatic residue in the external vestibule of the latter class of channels. Specifically, high-affinity block requires the presence a Tyr or Phe at position 401 in the pore loop of domain DI of the rat $Na_V1.4$ channel from skeletal muscle (9–11). We set out here to measure the energetic contribution of a potential cation-π interaction between TTX and the aromatic face of residue 401. A substantial cation-π interaction would provide insight into both the orientation of this residue in the extracellular mouth of the channel and of TTX in its blocking site. To this end, we substituted electron-withdrawing fluorine atoms for hydrogen atoms on the aromatic ring of residue 401, creating a series of fluorinated analogues of Phe. The functional equivalence of Phe and Tyr at the 401 position with respect to TTX block (Table 2) allows us to employ analogs of Phe in our analysis.

An energy-minimized structure (*A*) and the color-coded electrostatic potential (*B*) of TTX are shown in Fig. 1. Although

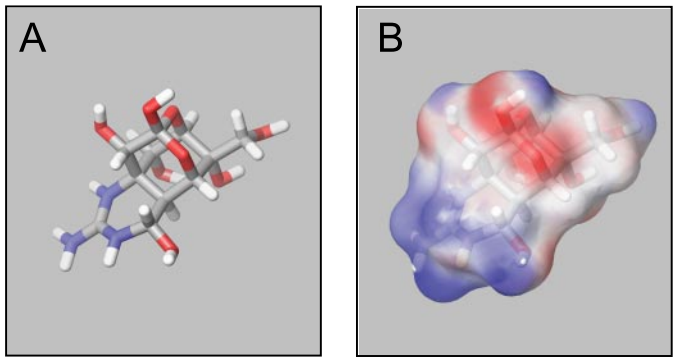

FIGURE 1. **Structure of TTX.** *A*, energy-minimized structure; *B*, surface rendering of TTX with electrostatic potential ranging from +100 kcal/mol (*blue*) to +40 kcal/mol (*red*). Note that the delocalized charge of TTX presents a substantial dipole moment, with positive potential concentrated near the guanidinium moiety.

a monovalent cation at neutral pH, TTX also has a large dipole moment of ~10 D, with an excess of positive charge (blue) near the guanidinium group. This would be expected to affect the orientation of TTX because of electrostatic interactions with its binding site.

Fig. 2 shows representative examples of inward sodium currents elicited by depolarizations from −30 mV to +10 mV in 5-mV steps from a holding potential of −100 mV. The Y401F mutant (Fig. 2*A*) was constructed by standard site-directed mutagenesis, while the remaining panels show currents for mutations introduced by nonsense suppression in which the cRNA encoding for $Na_V1.4$ was identical, containing a UAG codon at position 401. Fig. 2, *B–E*, shows the similarity of sodium currents co-expressing this cRNA construct with suppressor tRNAs ligated to the indicated derivatives of Phe. The peak current-voltage relationships from the fluorinated unnatural amino acids resulted in less than 5-mV shifts in activation compared with wild-type channels (data not shown). Injection of $Na_V1.4$-401UAG cRNA without a complementary suppressor tRNA failed to produce sodium currents (Fig. 2*F*), allowing us to rule out enzymatic manipulation within the oocyte expression system resulting in the incorporation of unexpected and unwanted natural amino acids. As a further control, no sodium current was seen when a complementary tRNA lacking an appended amino acid was co-injected with the $Na_V1.4$-401UAG cRNA.

Fig. 3 demonstrates the effect of serial fluorination at Phe^{401} on TTX affinity. The red traces from the same cells were recorded in the presence of the indicated concentrations of TTX. The six panels show currents for a variety of mutations at position 401 of $Na_V1.4$. Consistent with a cation-π interaction, increasing fluorination of residue Phe^{401} correlates with a decreased affinity for TTX block, as shown by the TTX concentration ([TTX]) required to reduce the current moderately in each mutant. *Insets* in Fig. 3 show the indicated aromatic rings of the unnatural amino acids as color-coded electrostatic potentials. Note that serial fluorination reduces the negative electrostatic potential (*red*) on the aromatic face with a minimal change in the overall structure.

Extracellular block of sodium channels by TTX is use-dependent, with repeated stimulation enhancing TTX affinity

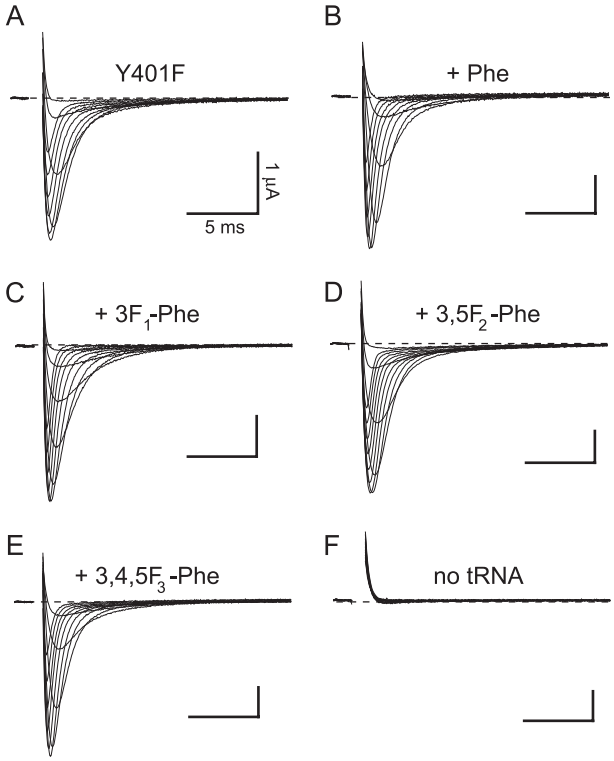

FIGURE 2. **Representative current traces from either Y401F or channels constructed from co-injection of Y401UAG cRNA with a complementary tRNA appended with the indicated amino acid.** Families of sodium currents are shown from depolarizations from −30 mV to +10 mV in 5-mV increments and were elicited from a holding potential of −100 mV. The voltage dependence and kinetics of currents of the Y401F point mutation (*A*) are indistinguishable from those of both natural and unnatural substitutions (*B–E*). Note the absence of currents upon injection of $Na_V1.4$ Y401UAG cRNA alone. *Scale bars* in each case are 5 ms and 1 μA.

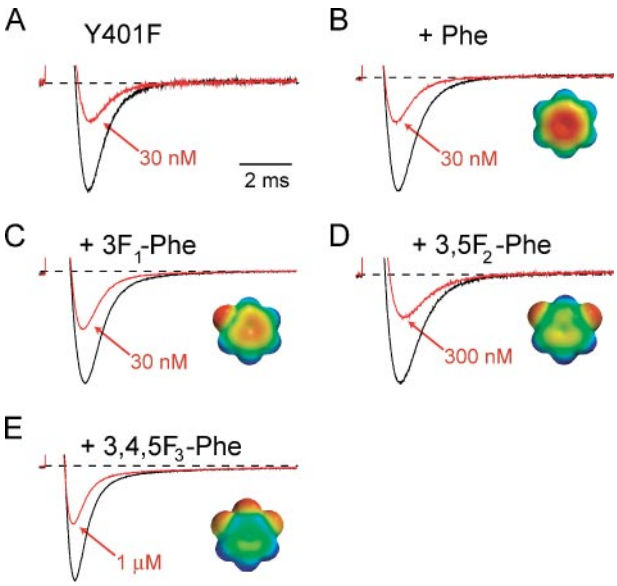

FIGURE 3. **Fluorination of Phe^{401} reduces TTX block.** Normalized currents recorded during a 10-ms depolarization to −10 mV from a holding potential of −100 mV. Control (bath) traces in *black*, and TTX at the labeled concentration in *red*. As Phe is fluorinated sequentially, a higher [TTX] is required for channel block. The *insets* represent electrostatic potentials of benzene with *red* negative (−20 kcal/mol), *blue* positive (+20 kcal/mol), and *green* neutral. Before normalization the peak inward currents were (in μA): Y401F, −1.92; Phe, −3.75; $3F_1$-Phe, −3.72; $3,5F_2$-Phe, −2.43; $3,4,5F_3$-Phe, −5.29.

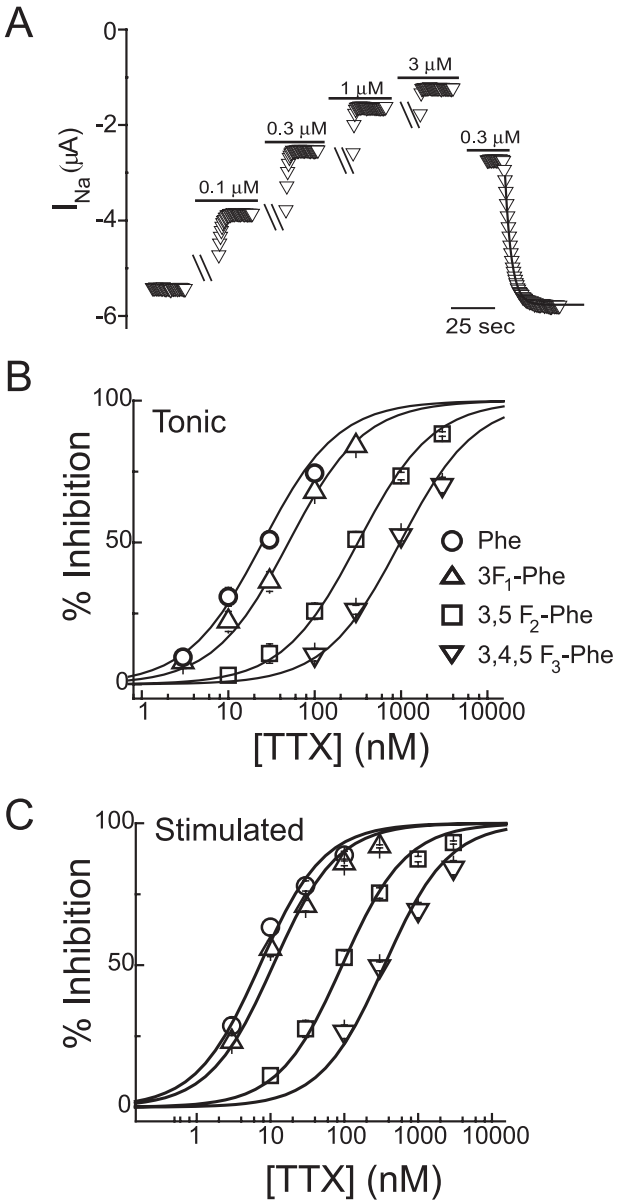

FIGURE 4. **Effect of fluorination on the dose-response relationship for TTX block.** *A*, cumulative dose-response experiment and washout of TTX for sodium currents with 3,4,5F_3-Phe at the 401 position. Peak currents simulated at 2 Hz in the presence of bath alone or bath plus TTX. 3 min were given between concentration exchange and stimulation, allowing the channels to recover to the tonic state (represented as hash marks). Rates and equilibrium constants of block (Table 2) were determined as described under "Experimental Procedures." In most cases a full dose-response relationship was obtained for each oocyte. The washout rates were fit well by a single exponential relaxation. *B*, TTX inhibition of $Na_v1.4$ in the tonic state. *C*, TTX inhibition of $Na_v1.4$ in the stimulated high affinity state.

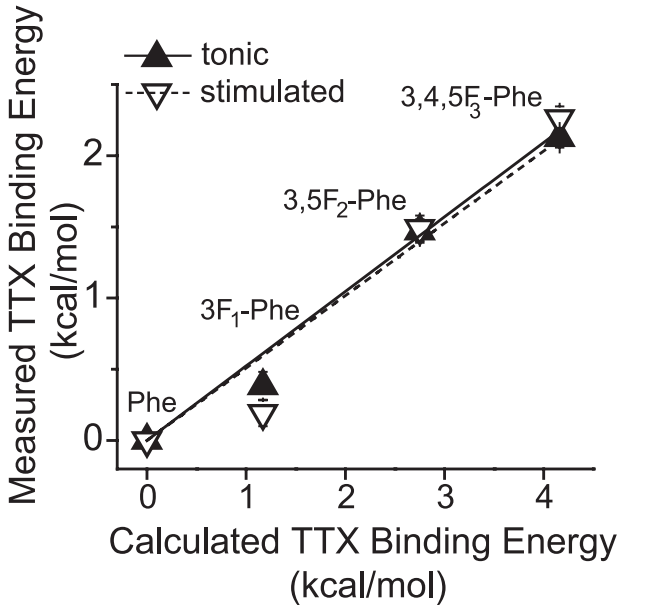

FIGURE 5. **Effect of fluorination on free energy of TTX binding.** TTX binding energy relative to unfluorinated Phe^{401} is plotted against the calculated TTX binding energy between TTX and a benzene ring (see "Experimental Procedures" and Table 1). Fluorinating the aromatic ring monotonically increases the relative free energy of the bound state. The change in binding energy is nearly identical for both the low and high affinity states, linear slopes of 0.52 and 0.51, respectively.

(35). This has been suggested to be due to electrostatic repulsion between TTX and a trapped Na^+ or Ca^{2+} ion within the pore, which is relieved when the trapped ion is released upon channel opening (7, 30, 35). Fig. 4*A* shows an example of a dose-response experiment that reveals both tonic (low affinity) and stimulated (high affinity) inhibition for the trifluorinated Phe derivative 3,4,5F_3-Phe. For each TTX concentration, the experiment consists of recording the current resulting from 100 depolarizations, each a 10-ms depolarization to −10 mV given at 2 Hz after a 3-min application of TTX. The first pulse in the train is used for determining the tonic inhibition, whereas the current elicited by the 100th pulse provides the stimulated block. TTX is perfused at the next higher concentration for 3 min to allow for the stimulated, TTX-bound state to re-equilibrate into the low affinity tonic state (30). After application of the highest [TTX], we return to a concentration close to the inhibition constant K_i of block, in this case 0.3 μM. Under continuous 2-Hz stimulation to hold blocked channels in the stimulated state, TTX is removed from the bath altogether. The time-dependent increase of current during washout is fit with a single exponential relaxation, which provides an estimate of the first order dissociation rate constant k_{off}^{H} for the high affinity-stimulated state. In Fig. 4, *B* and *C*, we show inhibition plots for the indicated amino acids in the tonic and stimulated states, respectively. Each data set is fit by a single binding isotherm with a Hill coefficient of 1. The trend for each condition is that serial reduction in electrostatic potential from the face of the aromatic ring at residue 401 leads to a monotonic increase in the inhibition constant K_i (Table 2), with the trifluorinated derivative increasing K_i by ~50-fold. Although the stimulated state consistently shows a higher affinity for TTX, both states are similarly affected by fluorination.

Estimates of rate constants for TTX block derived from these experimental data are shown in Table 2. The association rate constant (k_{on}) undergoes a ~17-fold decrease as residue 401 is converted from Phe to 3,4,5F_3-Phe, whereas the dissociation rate constant (k_{off}) increases ~3-fold. The general direction of the change in each rate constant is consistent with the progressive loss in TTX affinity with successive fluorination. Fig. 5 shows the effect of fluorination on TTX binding energies derived from experimental K_i values, plotted against the relative TTX binding energies obtained from an *ab initio* model of

TTX binding to an increasingly fluorinated benzene ring (see "Experimental Procedures" and Table 1). Consistent with a cation-π interaction, each added fluorine results in a stepwise increase in the relative free energy of the TTX-bound state, for both the experimental results and the theoretical model. The identical effect of fluorination on both tonic and stimulated states strongly suggests that both states involve the same physical interaction between TTX and the channel. The higher affinity of the stimulated state therefore represents a separate contribution to the binding energy, independent of the cation-π interaction we have been testing. A parsimonious interpretation of the data is that the nanomolar affinity of TTX for $Na_V1.4$ depends in part on a substantial cation-π interaction with an aromatic side chain at position 401.

DISCUSSION

Guanidinium toxins like TTX are potent blockers of voltage-gated sodium channels and have been invaluable both in the cloning of sodium channels (36, 37) and in the exploration of mechanisms of cation permeation. Early studies proposed a model whereby the guanidinium moiety of TTX acts as a mimic of a Na^+ ion and blocks at the outer entrance to the selectivity filter (38, 39). In the absence of an atomic structure of a sodium channel, the TTX binding site with its numerous contact points has been helpful in modeling both the external vestibule and the selectivity filter of voltage-gated sodium channels. Many such pore models are based on existing potassium channel structures which are refined further by consideration of the sodium channel point mutations that affect permeation and pore block (1, 33, 40–42). Among the extracellular residues that affect toxin block, position 401 ($Na_V1.4$ numbering) plays a unique role in discriminating between TTX-sensitive and TTX-resistant channels (8–11). Only TTX-sensitive channels have an aromatic residue (Phe or Tyr) at this position. Other residues in the extracellular vestibule of the pore, especially charged residues, may affect TTX block dramatically when mutated, but they tend to be highly conserved among all sodium channel isoforms. Although the importance of a Phe or Tyr residue at this discriminatory site is agreed upon universally, its energetic contributions to TTX binding and the precise nature of the TTX-aromatic interaction are not well understood. We set out to test whether an electrostatic cation-π interaction involving residue 401 contributes to TTX binding energy. Because an optimal cation-π interaction requires a close approach of the cation to the face, not the edge, of the aromatic ring, evidence for such an interaction adds another layer of structural information, in that the aromatic must orient appropriately toward the permeation pathway where it may interact electrostatically with cationic pore blockers and permeant cations alike.

The strategy we employed to test for a cation-π interaction, successive fluorination of the aromatic ring, is well established (22–26, 43) and based upon the fact that the predominant consequence of fluorine substitution is to decrease the negative electrostatic potential on the face of the aromatic residue. The predicted outcome of this manipulation for a cation-π interaction is a monotonic decrease in binding affinity, a result which is in complete accord with our data. As expected for a cation-π interaction, each added fluorine impacts K_i with a roughly equal increase in the free energy of binding (Fig. 5). The magnitude of the effect, ~2.2 kcal/mol for trifluorinating the aromatic ring, is roughly half that observed in previous studies of cationic ligands binding to aromatic residues in ion channels (23, 24, 26). This may be a consequence of the delocalized charge of the relatively large TTX molecule, which would tend to reduce its electrostatic attraction to the aromatic ring. Although essential to high affinity block, the cation-π component of binding cannot account for all of the binding energy. This is evident from an examination of the consequence of trifluorinating Phe^{401}. Earlier studies showed that trifluorobenzene is a good model for an aromatic that has little or no electrostatic binding ability (44, 45). Our data show that trifluorination of Phe^{401} still results in a channel with low micromolar affinity for TTX (Table 2) showing that, besides a cation-π interaction, other energetic components contribute to block.

To explore a hydrophobic contribution to TTX binding, we replaced Phe^{401} with Leu, a side chain that is structurally distinct from Phe yet is slightly more hydrophobic (46). The Y401L mutant has a comparable affinity for TTX as that of the trifluorinated derivative of Phe, 2.1 μM *versus* 0.97 μM, respectively, in the tonic state (Table 2). This result suggests that the 50-fold increase of K_i caused by trifluorinating Phe^{401} is due primarily to a loss of an electrostatic cation-π interaction. Note also that the effects of these two mutations are in stark contrast to the dramatic loss of TTX affinity seen by replacement with more polar amino acids such as Cys with a K_i of 108 μM (Table 2) or Glu with a K_i of 170 μM (8). This result may seem surprising at first glance, especially given that the monopole negative charge of Glu might be expected to attract a cation at least as well as the quadrupole potential on the aromatic face of Phe. For example, in the extracellular mouth of sodium channels a highly conserved ring of four acidic residues, two glutamates and two aspartates, produces a negative electrostatic potential in excess of −100 mV (15). This potential is believed to attract both permeant cations and positively charged blockers like TTX. An additional Glu at position 401 might also be expected to attract TTX electrostatically. Why, then, does the Y401E mutation reduce the affinity of TTX binding?

For binding to be optimal, there has to be a balance between the electrostatic attraction between the toxin and the side chain, and the energies of hydration of both TTX and its binding site (47, 48). Certainly, the dehydration cost is much less for an aromatic side chain than for the anionic Glu. As such, the innately weaker electrostatic interaction between TTX and the aromatic ring could, after considering solvation, contribute more to binding than the intrinsically stronger attraction between TTX and the carboxylate moiety of Glu (32). Thus, although the negative electrostatic potential of Glu could increase the local concentration of TTX in the extracellular vestibule of the pore, an intimate interaction is precluded by the inability of TTX to dehydrate the carboxylate. By contrast, a water-excluding contact between TTX and the aromatic would be able to not only attract but also orient the TTX molecule, which may account for the aromatic's advantage over an anionic side chain. Although this thermodynamic principle may account in part for the TTX preference for Tyr or Phe over Glu, it is not clear whether this argument

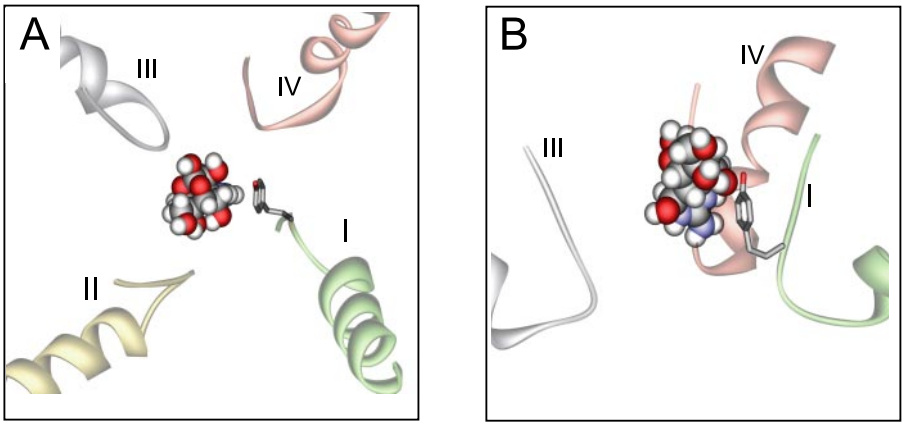

FIGURE 6. **Model of TTX docking in the pore mouth of $Na_v1.4$.** *A*, *top view* of TTX interacting with the pore loops of domains DI-DIV in the Lipkind-Fozzard model (33). This structure represents one possible configuration of the encounter complex. Note the guanidinium group of TTX in perpendicular apposition with the face of the aromatic ring of Tyr^{401}. *B*, *side view* of TTX in the pore.

can explain the low affinity for the Y401C mutant or whether, for example, some mutations of this residue produce local conformational changes that disrupt TTX binding. Evidence for this possibility is that the Y401C mutant loses its use dependence (Table 2). The possibility of conformational disruption of the binding site does not, however, invalidate our use of fluorinated Phe side chains because of the subtle nature of the mutations, by comparison with Y401C for example, and the simple monotonic relationship between TTX binding energy and the number of fluorine atoms substituted onto the aromatic ring (Fig. 5).

The effect of fluorination at Phe^{401} was identical for the tonic and stimulated states in both the trend and magnitude of binding free energy (Fig. 5). Although few molecular details are available on the use-dependent mechanism of TTX block, this result suggests that the critical TTX-aromatic complex has the same structure in both states. The different affinities of the tonic and stimulated states are therefore due to other energetic factors, such as the electrostatic repulsion between the toxin and cations trapped within the permeation pathway (30, 35).

Our kinetic analysis reveals that withdrawing electrostatic potential from the aromatic face of Phe^{401} affects the association rate constant k_{on} of TTX block more than its dissociation rate constant k_{off} (Table 2). A similar conclusion was reached previously by conventional mutagenic analysis of this and most other residues in the external vestibule. That is, reduction of TTX affinity often (but not always) involves a reduction of k_{on} rather than an increase of k_{off} (7, 8). The explanation for the asymmetric effects of such substitutions on these two rate constants is not clear, but might indicate that TTX block is a multistep process involving an initial association with the extracellular pore vestibule, including Phe^{401}, followed by a subsequent plugging of the pore. This possibility has been advanced in other studies of channel inhibitors in which association rates are more sensitive than dissociation rates to mutations (49, 50). This possibility is further supported by the fact that k_{on} for TTX block is well below the Smoluchowski limit expected for diffusional collision between a small blocker and an ion channel (51), indicating that the observed blocking rate is not diffusion-limited.

The role of a cation-π interaction in the blocking equilibrium is clear (Fig. 5), whether a TTX-aromatic complex is involved in the blocked state or in a transient intermediate. The blocked state itself likely includes hydrogen bonds and other short-range interactions. Also, a recent study of toxin block of a potassium channel raises the possibility that the conformation of the binding site and toxin might both change when the toxin binds (52).

In Fig. 6 we visualize a snapshot of one possible configuration of the encounter between TTX and Tyr^{401}. We used the coordinates of the pore mouth for $Na_V1.4$ from the model of Lipkind and Fozzard (33). In an alternative model the aromatic ring of Tyr^{401} was not oriented to face the permeation pathway (53) and was therefore inconsistent with the data in this article. To model the configuration in Fig. 6, we first optimized the structure of TTX and its minimum-energy conformation in complex with benzene, using high level *ab initio* calculations. The benzene of this complex was then aligned with the aromatic ring of Tyr^{401}. Because of the 6-fold symmetry of the ring, there are 6 possible orientations of the TTX-benzene complex with Tyr^{401}. The minimum energy orientation was estimated using molecular mechanics and then further refined using mixed-mode QM/MM. This structure is shown from above (Fig. 6*A*) and from the side (Fig. 6*B*). Notice that the guanidinium group, besides being in close apposition to the aromatic face of Tyr^{401}, is pointed downward toward the deeper residues of the selectivity filter. Further study will reveal whether this complex prevents Na^+ ion flux, either sterically or electrostatically, or whether the blocked state involves a subsequent movement of the toxin into a deeper position where it would plug the pore. Our model of block nevertheless supports the idea that a fundamental role of the TTX-aromatic interaction is to orient the toxin optimally to block the channel.

The conclusions of the present study are 3-fold. First, we demonstrate that the high affinity TTX block supported by an aromatic at position 401 is energetically based on a cation-π interaction between the TTX and the aromatic face of the side chain. These results therefore serve to answer a long standing puzzle regarding the conserved nature of a pore domain aromatic in high affinity sodium channel isoforms. Secondly, we show that the side chain at Tyr^{401} presents its aromatic face toward the permeation pathway where it can interact favorably with TTX and other cations. These results place geometric constraints on this side chain both in current structural models and in future atomic level structures of the sodium channel pore. Lastly, our results represent the first application of the *in vivo* nonsense suppression method for the incorporation of unnatural amino acids into a voltage-gated sodium channel. This work therefore serves as proof-of-principle to pave the way for future experiments utilizing this powerful technique to explore a variety of structural and mechanistic issues concerning

sodium channels, including the energetics that underlie cationic blockade by anti-arrhythmia, anti-epilepsy, and analgesic drugs.

Acknowledgments—We thank Mary Y. Ryan for help with oocytes and molecular biology. We also thank Drs. Lipkind and Fozzard for helpful discussions about TTX block.

REFERENCES

1. Dudley, S. C., Jr., Chang, N., Hall, J., Lipkind, G., Fozzard, H. A., and French, R. J. (2000) *J. Gen. Physiol.* **116,** 679–689
2. Yu, F. H., and Catterall, W. A. (2003) *Genome. Biol.* **4,** 207
3. Goldin, A. L., Barchi, R. L., Caldwell, J. H., Hofmann, F., Howe, J. R., Hunter, J. C., Kallen, R. G., Mandel, G., Meisler, M. H., Netter, Y. B., Noda, M., Tamkun, M. M., Waxman, S. G., Wood, J. N., and Catterall, W. A. (2000) *Neuron* **28,** 365–368
4. Noda, M., Suzuki, H., Numa, S., and Stühmer, W. (1989) *FEBS Lett.* **259,** 213–216
5. Terlau, H., Heinemann, S. H., Stühmer, W., Pusch, M., Conti, F., Imoto, K., and Numa, S. (1991) *FEBS Lett.* **293,** 93–96
6. Kontis, K. J., and Goldin, A. L. (1993) *Mol. Pharmacol.* **43,** 635–644
7. Boccaccio, A., Moran, O., Imoto, K., and Conti, F. (1999) *Biophys. J.* **77,** 229–240
8. Penzotti, J. L., Fozzard, H. A., Lipkind, G. M., and Dudley, S. C., Jr. (1998) *Biophys. J.* **75,** 2647–2657
9. Satin, J., Kyle, J. W., Chen, M., Bell, P., Cribbs, L. L., Fozzard, H. A., and Rogart, R. B. (1992) *Science* **256,** 1202–1205
10. Chen, L.-Q., Chahine, M., Kallen, R. G., Barchi, R. L., and Horn, R. (1992) *FEBS Lett.* **309,** 253–257
11. Backx, P. H., Yue, D. T., Lawrence, J. H., Marban, E., and Tomaselli, G. F. (1992) *Science* **257,** 248–251
12. Heinemann, S. H., Terlau, H., Stühmer, W., Imoto, K., and Numa, S. (1992) *Nature* **356,** 441–443
13. Schlief, T., Schönherr, R., Imoto, K., and Heinemann, S. H. (1996) *Eur. Biophys. J.* **25,** 75–91
14. Chiamvimonvat, N., Pérez-García, M. T., Tomaselli, G. F., and Marban, E. (1996) *J. Physiol.* **491,** 51–59
15. Hui, K., McIntyre, D., and French, R. J. (2003) *J. Gen. Physiol.* **122,** 63–79
16. Chiamvimonvat, N., Pérez-García, M. T., Ranjan, R., Marban, E., and Tomaselli, G. F. (1996) *Neuron* **16,** 1037–1047
17. Favre, I., Moczydlowski, E., and Schild, L. (1996) *Biophys. J.* **71,** 3110–3125
18. Ma, J. C., and Dougherty, D. A. (1997) *Chem. Rev.* **97,** 1303–1324
19. Gallivan, J. P., and Dougherty, D. A. (1999) *Proc. Natl. Acad. Sci. U. S. A.* **96,** 9459–9464
20. Dougherty, D. A. (1996) *Science* **271,** 163–168
21. Nowak, M. W., Gallivan, J. P., Silverman, S. K., Labarca, C. G., Dougherty, D. A., and Lester, H. A. (1998) *Methods Enzymol.* **293,** 504–529
22. Zhong, W. G., Gallivan, J. P., Zhang, Y. N., Li, L. T., Lester, H. A., and Dougherty, D. A. (1998) *Proc. Natl. Acad. Sci.* **95,** 12088–12093
23. Beene, D. L., Brandt, G. S., Zhong, W., Zacharias, N. M., Lester, H. A., and Dougherty, D. A. (2002) *Biochemistry* **41,** 10262–10269
24. Lummis, S. C., Beene, D. L., Harrison, N. L., Lester, H. A., and Dougherty, D. A. (2005) *Chem. Biol.* **12,** 993–997
25. McMenimen, K. A., Petersson, E. J., Lester, H. A., and Dougherty, D. A. (2006) *ACS Chem. Biol.* **1,** 227–234
26. Ahern, C. A., Eastwood, A. L., Lester, H. A., Dougherty, D. A., and Horn, R. (2006) *J. Gen. Physiol.* **128,** 649–657
27. Leo, A., Hansch, C., and Elkins, D. (1971) *Chem. Rev.* **71,** 525–616
28. Nowak, M. W., Kearney, P. C., Sampson, J. R., Saks, M. E., Labarca, C. G., Silverman, S. K., Zhong, W., Thorson, J., Abelson, J. N., Davidson, N., Schultz, P. G., Dougherty, D. A., and Lester, H. A. (1995) *Science* **268,** 439–442
29. Cannon, S. C., McClatchey, A. I., and Gusella, J. F. (1993) *Pflugers* **423,** 155–157
30. Conti, F., Gheri, A., Pusch, M., and Moran, O. (1996) *Biophys. J.* **71,** 1295–1312
31. Moran, O., Picollo, A., and Conti, F. (2003) *Biophys. J.* **84,** 2999–3006
32. Gallivan, J. P., and Dougherty, D. A. (2000) *J. Am. Chem. Soc.* **122,** 870–874
33. Lipkind, G. M., and Fozzard, H. A. (2005) *Mol. Pharm.* **68,** 1611–1622
34. Kaminski, G. A., Friesner, R. A., Tirado-Rives, J., and Jorgensen, W. L. (2001) *J. Phys. Chem. B* **105,** 6474–6487
35. Salgado, V. L., Yeh, J. Z., and Narahashi, T. (1986) *Ann. N. Y. Acad. Sci.* **479,** 84–95
36. Noda, M., Shimizu, S., Tanabe, T., Takai, T., Kayano, T., Ikeda, T., Takahashi, H., Nakayama, H., Kanaoka, Y., Minamino, N., Kangawa, K., Matsuo, H., Raftery, M. A., Hirose, T., Inayama, S., Hayashida, H., Miyata, T., and Numa, S. (1984) *Nature* **312,** 121–127
37. Noda, M., Ikeda, T., Kayano, T., Suzuki, H., Takeshima, H., Kurasaki, M., Takahashi, H., and Numa, S. (1986) *Nature* **320,** 188–192
38. Hille, B. (1971) *J. Gen. Physiol.* **58,** 599–619
39. Hille, B. (1975) *Biophys. J.* **15,** 615–619
40. Lipkind, G. M., and Fozzard, H. A. (2000) *Biochemistry* **39,** 8161–8170
41. Penzotti, J. L., Lipkind, G., Fozzard, H. A., and Dudley, S. C., Jr. (2001) *Biophys. J.* **80,** 698–706
42. Bruhova, I., and Zhorov, B. S. (2005) *Biophys. J.* **89,** 1020–1029
43. Morikubo, N., Fukuda, Y., Ohtake, K., Shinya, N., Kiga, D., Sakamoto, K., Asanuma, M., Hirota, H., Yokoyama, S., and Hoshino, T. (2006) *J. Am. Chem. Soc.* **128,** 13184–13194
44. Williams, J. H. (1993) *Accounts Chem. Res.* **26,** 593–598
45. Mecozzi, S., West, A. P., Jr., and Dougherty, D. A. (1996) *J. Am. Chem. Soc.* **118,** 2307–2308
46. Radzicka, A., Pedersen, L., and Wolfenden, R. (1988) *Biochem.* **27,** 4538–4541
47. Eisenman, G. (1962) *Biophys. J.* **2,** 259–323
48. Eisenman, G., and Horn, R. (1983) *J. Memb. Biol.* **76,** 197–225
49. Escobar, L., Root, M. J., and MacKinnon, R. (1993) *Biochemistry* **32,** 6982–6987
50. Shahidullah, M., Harris, T., Germann, M. W., and Covarrubias, M. (2003) *Biochemistry* **42,** 11243–11252
51. Camacho, C. J., Weng, Z., Vajda, S., and DeLisi, C. (1999) *Biophys. J.* **76,** 1166–1178
52. Lange, A., Giller, K., Hornig, S., Martin-Eauclaire, M. F., Pongs, O., Becker, S., and Baldus, M. (2006) *Nature* **440,** 959–962
53. Tikhonov, D. B., and Zhorov, B. S. (2005) *Biophys. J.* **88,** 184–197